This article has been accepted for inclusion in a future issue of this journal. Content is final as presented, with the exception of pagination.

HFSS and CST Simulations of a GW-Class MILO

Drew A. Packard, *Graduate Student Member, IEEE*, Anna Cooleybeck, Nicholas M. Jordan, *Senior Member, IEEE*, Brendan J. Sporer, Alexander E. Mazarakis, *Student Member, IEEE*, Y. Y. Lau, *Fellow, IEEE*, Ronald M. Gilgenbach, *Life Fellow, IEEE*, and Ryan D. McBride, *Member, IEEE*

***Abstract*— A magnetically insulated line oscillator (MILO) was studied using the simulation software packages high-frequency structure simulator (HFSS) and Computer Simulation Technology-Particle Studio (CST-PS). HFSS was used to find dispersion characteristics of the slow-wave structure and predict resonant-mode frequencies. CST-PS was used to analyze the operation of the device with space charge included. At an applied voltage of 500 kV, CST-PS predicted 1.25-gigawatt (GW) microwave generation at 1.2 GHz while drawing 57 kA. These simulations are consistent with previously published experimental results for a similar MILO. The CST-PS model was used to predict MILO operation as a function of injected voltage, and a separate study was performed to evaluate the effects of an independent, externally applied axial magnetic field. These simulation efforts are in support of upcoming experiments at the University of Michigan, where the MILO investigated in this article will be tested on a new linear transformer driver facility.**

***Index Terms*— Computer Simulation Technology-Particle Studio (CST-PS), dispersion relation, high power microwaves (HPMs), linear transformer driver (LTD), magnetically insulated line oscillator (MILO), particle in cell (PIC), pulsed power.**

I. Introduction

THE magnetically insulated line oscillator (MILO) [1]–[3] is a high-power microwave (HPM) source capable of generating up to gigawatt (GW) power levels [4]–[6]. Similar to the magnetron [7], the MILO is a crossed-field device. The MILO is a desirable HPM source because it generates a self-insulating magnetic field for interaction between a central cathode and surrounding anode slow-wave structure (SWS), enabling operation without external magnets. This allows the MILO to generate beam powers of up to tens of GWs without experiencing electrical breakdown across the anode–cathode (AK) gap. Because of its need for very large injected currents, the MILO is an inherently low-impedance device ($\sim$3 Ω).

HPM sources are often used in applications such as radar, signal jamming, and electronic warfare, to name a few [8]. In many of the avenues in which HPM is needed, the compactness, form factor, and total weight of the device are important considerations. The fact that the MILO requires no externally applied magnetic field gives it an advantage over other devices in these regards.

Another necessary consideration in HPM systems is the choice of pulsed power for driving the source. Typically, Marx generators have been used for MILO applications. A more recent innovation in pulsed power is the linear transformer driver (LTD) [9]–[12]. The LTD is a compact and efficient pulsed power technology used to drive high current and power at relatively low voltage and low impedance. The MILO is well matched to such a driver, and the LTD is capable of delivering the large input power necessary. The combination of the two could lead to one of the most compact, moderate voltage, GW-class HPM systems to exist.

As modern research continues to improve the MILO [13]–[15], investigators at the University of Michigan (UM) are assembling an LTD test bed to explore its capability to drive HPM sources. The first is likely to be a GW-class MILO, similar to the device studied by Haworth *et al.* [5] and Lemke *et al.* [6]. In preparation for these experiments, simulations were performed in high-frequency structure simulator (HFSS) and Computer Simulation Technology-Particle Studio (CST-PS) to compare with past experiments and benchmark the device using these more modern simulation packages. HFSS was used to find dispersion characteristics of the SWS, while CST-PS was used to analyze output power as a function of applied voltage, and to predict MILO operation in the presence of a modest, externally applied axial magnetic field.

II. HFSS Cold Test Simulations

Simulations of the MILO [5], [6], [16] were performed in HFSS to analyze the modes that exist in the SWS. This analysis was performed using both a full model of the SWS and a unit cell approach [17], [18], each of which are shown in Fig. 1. The MILO SWS is a corrugated cylindrical waveguide with vanes of various inner radii and unit cell length P. The longest vanes are labeled 1–3, while vanes 4–6 are of intermediate length, and vane 7 is the shortest.

In the full model, the SWS and cathode are assigned perfect electrical conductor (PEC) boundary conditions, forcing a normal electric field at every surface. The HFSS eigenmode solver was used to determine the resonant modes of this system. The unit cell model also applies PEC boundary conditions to the cathode and SWS, but an additional boundary condition is necessary at the open vacuum interface. This is satisfied with phase advance boundary conditions; at the opposing vacuum

Manuscript received November 15, 2019; revised March 7, 2020; accepted April 7, 2020. This work was supported in part by the U.S. Office of Naval Research through the Young Investigator Program and the Counter Directed Energy Weapons Program under Grant N00014-18-1-2499 and Grant N000014-19-1-2262. *(Corresponding author: Drew A. Packard.)*

The authors are with the Department of Nuclear Engineering and Radiological Sciences, University of Michigan, Ann Arbor, MI 48109 USA (e-mail: drupac@umich.edu).

Color versions of one or more of the figures in this article are available online at http://ieeexplore.ieee.org.

Digital Object Identifier 10.1109/TPS.2020.2990163

0093-3813 © 2020 IEEE. Personal use is permitted, but republication/redistribution requires IEEE permission.
See https://www.ieee.org/publications/rights/index.html for more information.

Authorized licensed use limited to: University of Michigan Library. Downloaded on May 12,2020 at 14:57:26 UTC from IEEE Xplore. Restrictions apply.

This article has been accepted for inclusion in a future issue of this journal. Content is final as presented, with the exception of pagination.

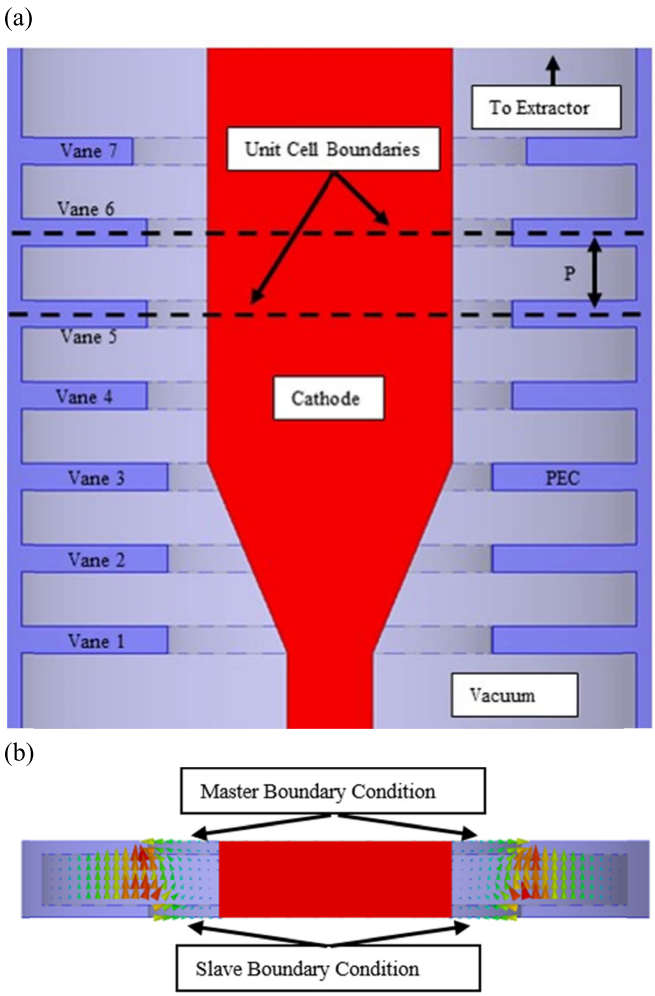

Fig. 1. HFSS models used for analyzing the SWS. (a) Full SWS. (b) Unit cell approach with the solved electric-field overlaid.

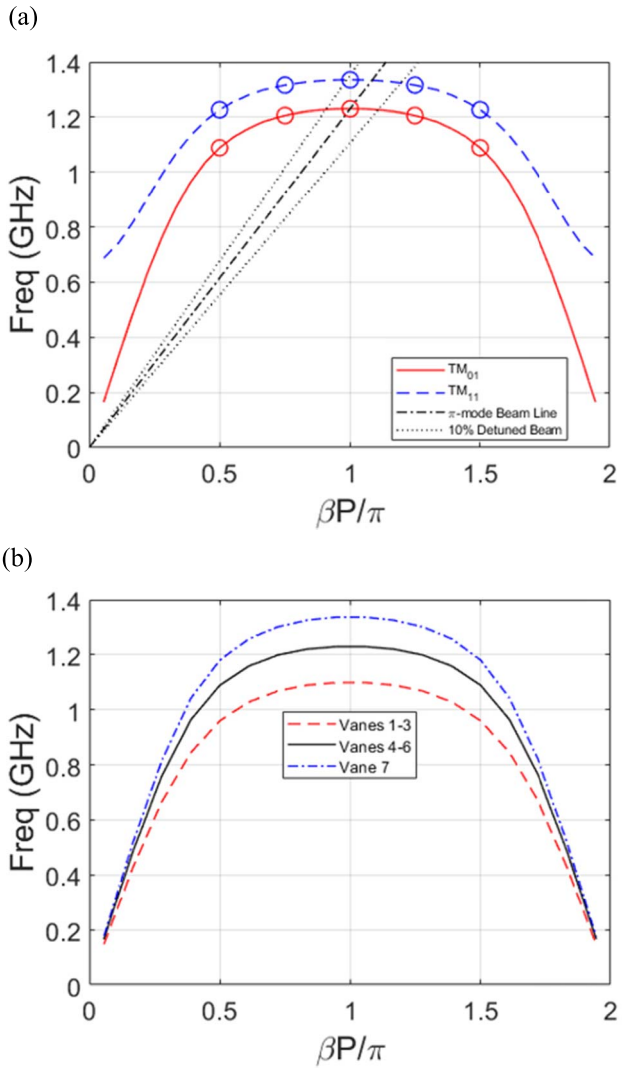

Fig. 2. Dispersion relations obtained with the unit cell method. (a) Fundamental circuit mode (TM_{01}) and the first higher order circuit mode (TM_{11}) in vanes 4–6. (b) Fundamental mode of each cavity structure.

interfaces, master-slave conditions are applied. This forces the electric field to advance a specified phase difference between the master and slave, and effectively turns the unit cell into a SWS of infinite length. By varying this phase difference, the dispersion relation for each section of the SWS and the various supported modes can be obtained.

The corrugated cylindrical waveguide supports a series of transverse magnetic (TM_{mn}) modes, where the integers m and n describe the variation in the field azimuthally and radially, respectively. The TM_{01} and TM_{11} modes are the lowest order field patterns supported by the MILO. The cavities between vanes 3 and 7 are where the SWS was designed to interact with the electron beam in the TM_{01} π-mode. Thus, the dispersion relations for the TM_{01} and TM_{11} modes within vanes 4–6 using the unit cell technique are plotted in Fig. 2(a) to examine the possibility of interaction with modes that were not intended. In addition, the relevant resonant mode frequencies of the four-cavity structure for both TM waves are overlaid with circles.

The model indicates that if a beam synchronous with the TM_{01} π-mode velocity is detuned by less than 10%, it could interact with the neighboring TM_{11} π-mode. Motion of charge in crossed field devices is dominated by Brillouin flow [19], [20], and therefore faster electrons in the shear flow extending further into the gap could excite this mode instead of the desired TM_{01} π-mode. The frequencies of the resonant modes supported by these TM waves in a four-cavity structure, calculated using the unit cell and full model method, are listed in Table I. To increase the frequency separation between the TM_{11} and TM_{01} modes, the vane inner radius can be reduced while maintaining the overall vane length.

Fig. 2(b) shows the dispersion relation for the different vane structures in the MILO. The TM_{01} π-mode, excited in

TABLE I

RELEVANT RESONANT FREQUENCIES OF THE TM_{01} AND TM_{11} MODES FOR VANES 4–6, OBTAINED FROM THE UNIT CELL AND FULL MODEL APPROACH

Mode	Unit Cell Model Frequency (GHz)		Full Model Frequency (GHz)	
	TM_{01}	TM_{11}	TM_{01}	TM_{11}
$\pi/2$	1.089	1.227	1.033	1.185
$3\pi/4$	1.206	1.316	1.166	1.277
π	1.231	1.335	1.220	1.320

Authorized licensed use limited to: University of Michigan Library. Downloaded on May 12,2020 at 14:57:26 UTC from IEEE Xplore. Restrictions apply.

This article has been accepted for inclusion in a future issue of this journal. Content is final as presented, with the exception of pagination.

vanes 4–6, is not allowed to propagate upstream due to the presence of the choke cavities between vanes 1–3 [21]. The TM_{01} π-mode is evanescent in the choke cavities, demonstrated by the dispersion relation of vanes 1–3. On the other hand, the fringing fields from the TM_{01} π-mode excite a traveling wave with positive group velocity at vane 7 in the direction of the coaxial output. Thus, reducing the length of vane 7 improves the impedance match between the SWS and the output.

Each of these approaches has its advantages and disadvantages. The full model will likely provide a more accurate prediction of experimental cold-test resonant-mode frequencies. However, this method requires a mesh for the entire device, which may be unnecessary. Furthermore, this method cannot be used to find the full dispersion relation for circuit modes on a SWS; it can only find the discrete resonant modes supported by the finite SWS. The unit cell approach is much faster, allowing for rapid prototyping and design. Because the unit cell model is an infinite SWS and the phase per cell can be controlled, it can be used to predict the dispersion relation of SWS modes relatively easily. Compared to the full model, the mode frequency estimates from the unit cell approach are accurate to first order. The remaining simulations in Section III were performed in CST-Particle Studio.

III. CST Particle Simulations

Fig. 3 shows the full CST-Particle Studio model of the MILO. The driver voltage is injected through a discrete port at the bottom of the device. The total injected current and voltage are measured by monitors residing between the input port and the cathode taper. Voltage monitors are placed in each cavity of the SWS to identify the dominant mode in each cavity. Explosive emission of electrons is allowed from the cylindrical portion of the cathode that resides above the taper. The vast majority of the current driven through the MILO is collected by the beam dump. This axial current sets up an azimuthal magnetic field that magnetically insulates the diode and allows for crossed field interactions in the SWS. The beam dump is dc-shorted to ground with three conducting rods located at discrete azimuthal locations; these three rods form a quarter-wave structure that is transparent to the microwaves. Finally, the traveling wave launched into the output coax by the final vane is absorbed by a perfectly matched boundary condition. The radio frequency (RF) current and voltage at the output are measured to determine the output power.

Fig. 4 shows the output characteristics of a CST-PS simulation of the MILO. A voltage of 500 kV is injected in the shape of a half sine wave over 300 ns, drawing 57 kA at peak current, and generating a peak power of 1.25 GW with 4.5% efficiency in the $TM_{01}\pi$-mode at 1.199 GHz. In previous experimental tests of an MILO similar to the one modeled in this article, a 500-kV drive voltage resulted in 1.5–2 GW of output power at 1.2 GHz while drawing approximately 60 kA [16].

Fig. 5 shows the peak output power of CST-PS MILO simulations as a function of the injected voltage for different mesh refinements and compares the prediction to

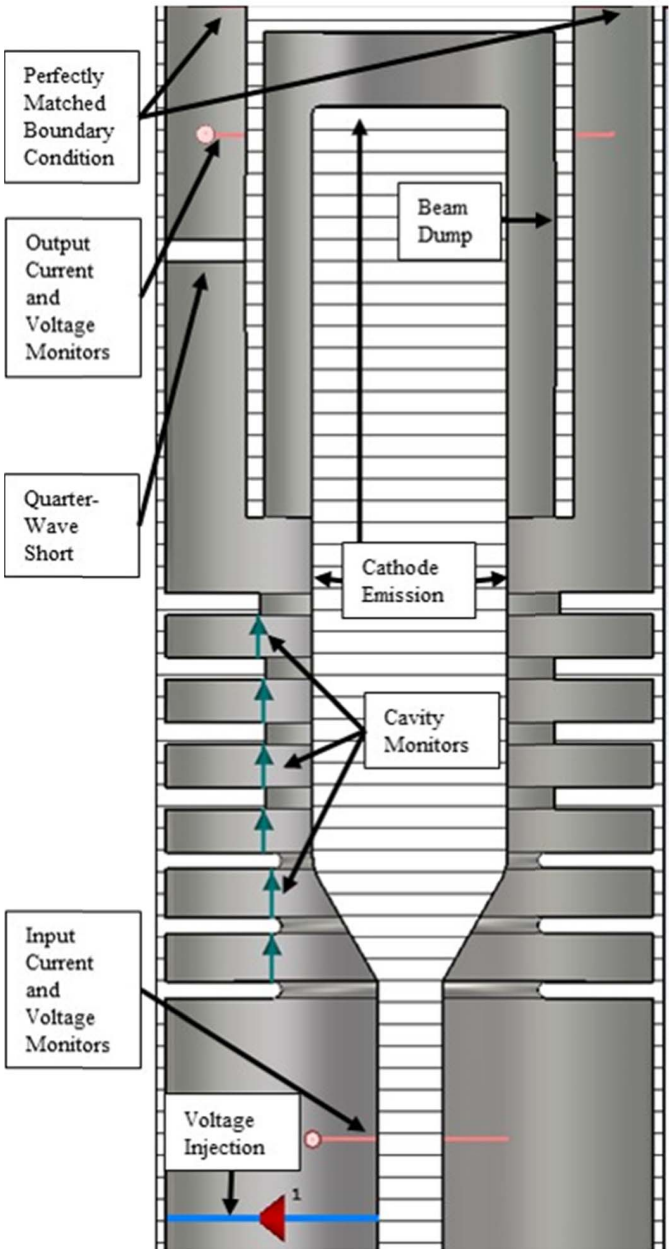

Fig. 3. Cross-sectional view of the MILO modeled in CST-Particle Studio.

past experiments of a similar MILO by Calico *et al.* [21]. While good agreement was observed for $V < 400$ kV, the simulation overpredicted output power for higher applied voltages. These were not, however, identical MILO geometries; the primary difference between the CST-PS model and the experimental data of Calico *et al.* [21] is the location of the cathode taper. In the CST-PS models, the cathode tapers under the choke vanes, whereas the tested prototype had its taper before the choke vanes. Subsequent MILO experiments demonstrated an increase in output power when the taper was placed beneath the choke vanes [16]. This increase in power was accredited to the elimination of unwanted emission on the cathode directly beneath the choke vanes.

At voltages less than 200 kV, CST-PS did not demonstrate operation in any mode in the SWS. This is in contrast with

Authorized licensed use limited to: University of Michigan Library. Downloaded on May 12,2020 at 14:57:26 UTC from IEEE Xplore. Restrictions apply.

This article has been accepted for inclusion in a future issue of this journal. Content is final as presented, with the exception of pagination.

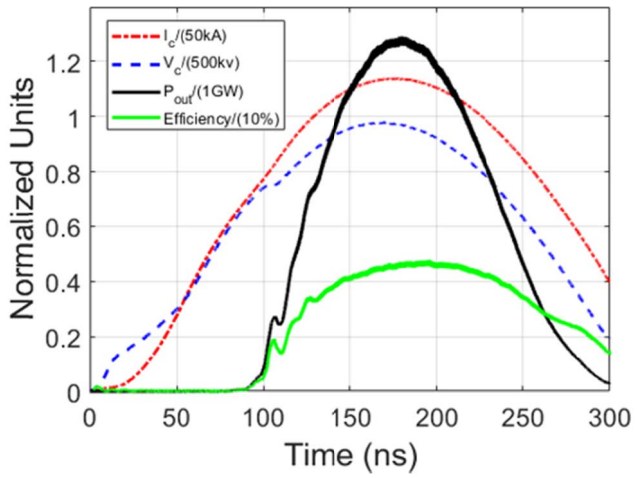

Fig. 4. Output power, efficiency, injected current, and cathode voltage for a CST-PS simulation over time.

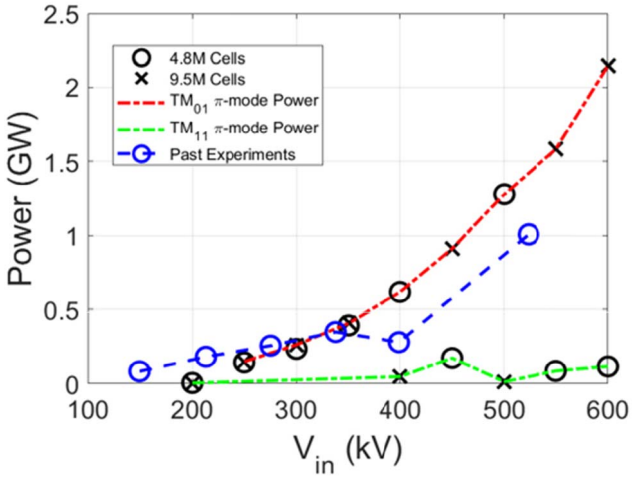

Fig. 5. Comparison of experimental [21] and simulated (this article) peak output power of the TM_{01} and TM_{11} π-mode as a function of injected voltage. The predicted operating mode is found to be dependent on mesh size.

the experiment, where generation of roughly 100 MW was observed at these voltages. It is assumed that at these low-electric fields, the simulated axial beam velocity is not fast enough to synchronize with a SWS mode. At 200 kV specifically, CST-PS predicted TM_{11} π-mode operation regardless of the mesh refinement, resulting in negligible power extraction. This is also in disagreement with experiment, where at 200-kV generation of approximately 200 MW in the TM_{01} π-mode was observed. From 250 to 350 kV, CST-PS calculated a near-linear relationship between voltage and output power, regardless of the mesh size. In this range, the simulated output power agrees with experiment.

From 400 to 600 kV, at a given voltage, the different mesh sizes do not yield the same dominant mode. For example, at 400 kV, the 4.8M-cell model (circles) predicts TM_{01} π-mode operation, generating 610 MW, while the 9.5M-cell model (crosses) predicts TM_{11} π-mode operation, resulting in very little power extraction. The TM_{01} (red) and TM_{11} (green) π-mode power connects all cases from both model resolutions that demonstrated operation of each respective mode. At each voltage in this range, the mesh sizes alternate in their prediction between these two modes, resulting in the data points with reduced power extraction. While this oscillatory behavior is not expected with increased mesh refinement, upon consideration of Fig. 2(a), it is not surprising the TM_{11} π-mode is dominant in some of these simulations.

Despite the inconsistency of mode prediction, it appears the TM_{01} π-mode power generation predicted by both models is in fact converged. That is, when considering only the TM_{01} π-mode data points in Fig. 5, the 4.8M-cell data points fall on the line of best fit retrieved from 9.5M-cell data. It is expected that with further mesh refinement, CST-PS will provide a more consistent prediction of the operating mode across the swept voltage, but the output power will not change significantly.

IV. Application of External Magnetic Fields

Early and late in the voltage pulse, magnetic insulation in the SWS is lost because the current driven through the beam dump is not sufficiently high to generate the Hull cutoff magnetic field. This causes unnecessary damage and destruction to the MILO SWS, and reduction of this thermal load could allow operation at higher duty cycles. Thus, the application of a modest, uniform axial magnetic field (B_z) to the MILO was studied using CST-PS. Such a magnetic field would provide insulation while the MILO is not generating RF. The goal of this article is to determine the feasibility of shielding the anode from unnecessary damage while not affecting the output power or efficiency. Application of an external magnetic field might also allow MILOs to be driven by higher impedance pulsed power generators.

Fig. 6 compares electron trajectories in the π-mode with and without B_z, each at an applied voltage of 500 kV. In Fig. 6(a), B_z is set to zero, and therefore the total magnetic field in the SWS region is purely azimuthal (φ). The electrons thus drift primarily in the z-direction due to the $\vec{E}_{\mathrm{DC}} \times \vec{B}_{\varphi}$ drift velocity, while also oscillating in the radial direction due to the RF drift $\vec{E}_{\mathrm{RF}} \times \vec{B}_{\varphi}$.

In Fig. 6(b), B_z is set to 0.05 T. Herein, the total magnetic field in the SWS region is a helical combination of the applied axial field and the self-generated azimuthal field. Consequently, electrons in the hub drift helically about the cathode as they stream off the cathode.

The microwave output power and efficiency for these simulations are shown in Fig. 7(a) and (b), respectively. At 500 kV, while π-mode operation is still achieved with B_z set to 0.05 T, the output power and efficiency decrease by approximately a factor of two from the nominal case. This is explained by reduced synchronism between the axial velocity of the helical beam and the SWS phase velocity.

In an effort to retrieve the lost efficiency, B_z was held at 0.05 T and the voltage was raised to 700 kV to increase the axial velocity of the hub back to a more synchronous state with the SWS. This resulted in increased power generation due to the higher voltage, and the efficiency was found to be within 10% of that for the nominal case [see Fig. 7(a) and (b), respectively]. Furthermore, the output frequency was not significantly affected by the external magnetic field. In the:

Authorized licensed use limited to: University of Michigan Library. Downloaded on May 12,2020 at 14:57:26 UTC from IEEE Xplore. Restrictions apply.

This article has been accepted for inclusion in a future issue of this journal. Content is final as presented, with the exception of pagination.

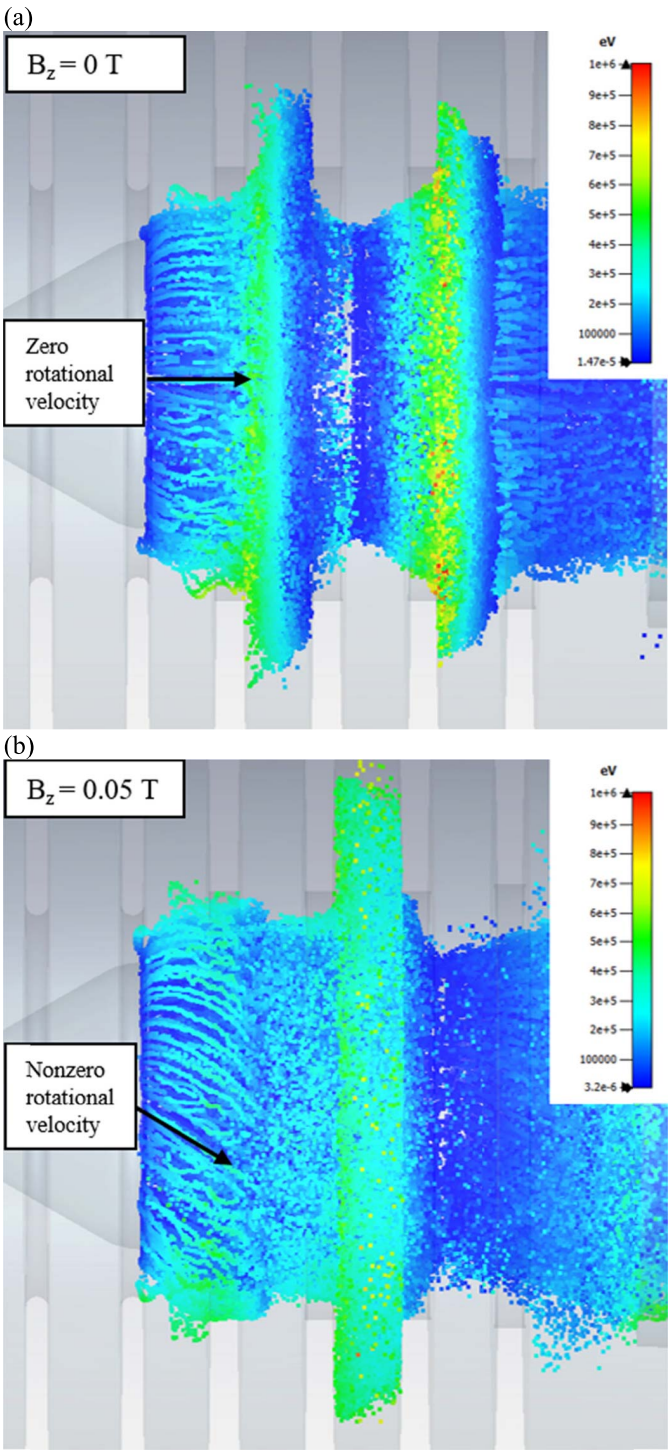

Fig. 6. Electron trajectories in the MILO SWS for an applied axial magnetic field of (a) 0 T and (b) 0.05 T. It is noted that π-mode operation is observed in both cases, and that helical electron trajectories are observed in (b).

1) 500 kV, 0 T; 2) 500 kV, 0.05 T; and 3) 700 kV, 0.05 T cases, the output frequencies were: 1) 1.199; 2) 1.1915; and 3) 1.193 GHz, respectively. Thus, it appears that applying an axial magnetic field in an MILO, to reduce potential damage to the SWS, might not adversely affect microwave generation if accounted for correctly. Successful application of an axial magnetic field requires accurate prediction of the axial hub velocity in the helical flow for correct interaction with the SWS wave.

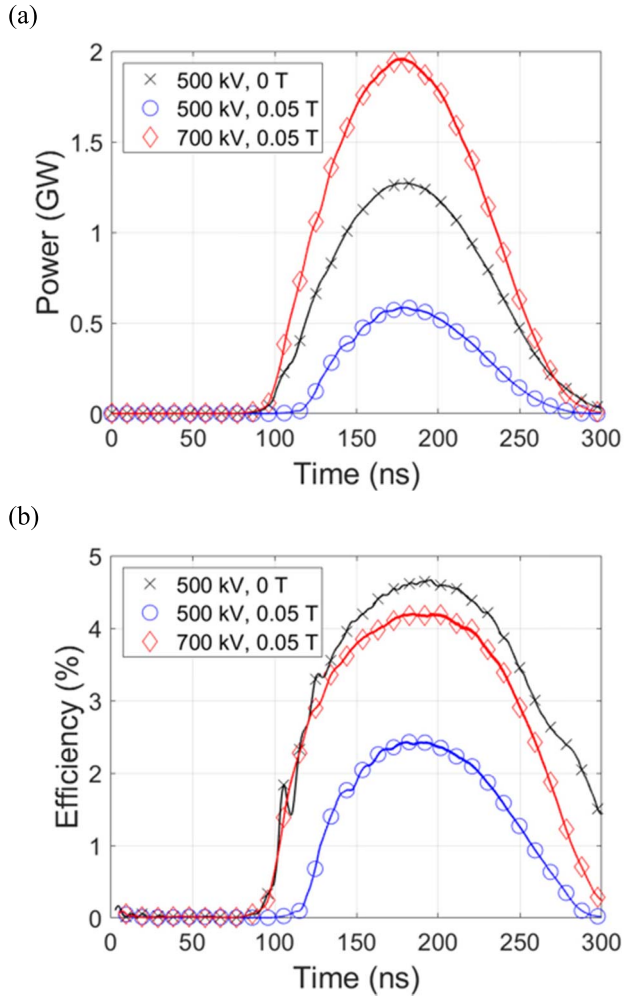

Fig. 7. (a) Simulated power and (b) efficiency plotted as a function of time for different voltages and applied magnetic fields.

V. Future Experimental Plans

A new pulsed-power facility called Bestowed LTD from the Ursa-Minor Experiment (BLUE) is presently under construction at UM. BLUE will consist of up to four 1.25-m diameter LTD cavities stacked together in series. These four cavities were originally part of the 21-cavity Ursa Minor facility at Sandia National Laboratories [22], [23]. A single LTD cavity is a low-impedance driver. By stacking multiple cavities together in series, both the driver voltage and the driver impedance is increased in proportion to the number of cavities used [9]. BLUE is being configured such that one, two, three, or four cavities can be used in series, thus allowing the driver impedance to be tuned to better match a given load. A single fully populated BLUE cavity has a driver impedance of about 0.5 Ω. Thus, the four-cavity BLUE system will have a driver impedance of approximately 2 Ω, which should be well matched to MILO loads (∼3 Ω). We note that driving an HPM load with an LTD has received limited attention in the literature [24]. Furthermore, to our knowledge,

Authorized licensed use limited to: University of Michigan Library. Downloaded on May 12,2020 at 14:57:26 UTC from IEEE Xplore. Restrictions apply.

This article has been accepted for inclusion in a future issue of this journal. Content is final as presented, with the exception of pagination.

(a)

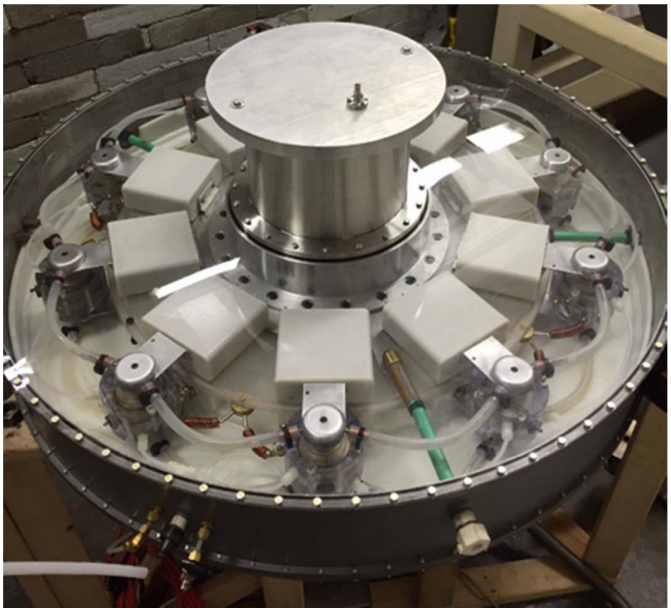

(b)

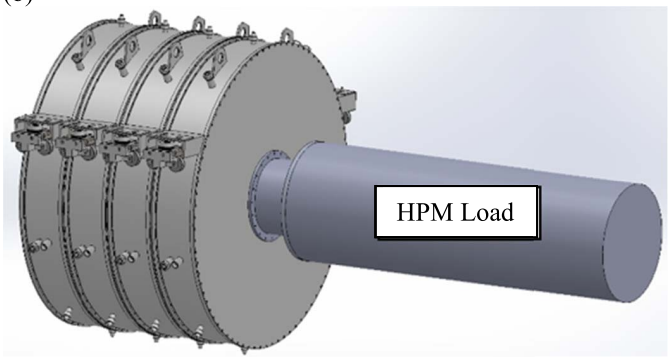

Fig. 8. Photographs and images of the hardware to be tested in upcoming experiments at UM. (a) Photograph of the first fully populated BLUE LTD cavity. (b) CAD model of BLUE's four LTD cavities stacked in series, forming a four-cavity LTD module, and connected to the GW-class MILO (labeled "HPM load").

(c)

Fig. 8. *(Continued.)* (c) Brazed GW-class MILO to be tested experimentally on the BLUE LTD facility.

no experimental tests of an LTD-driven MILO have been reported in the literature. Thus, preparations are underway to test a GW-class MILO on BLUE.

Fig. 8 depicts the hardware that will be tested in upcoming experiments at UM. In Fig. 8(a), a photograph of the first fully populated BLUE cavity is shown. Because of the clear plastic lid, the interior components are visible (switches, capacitors, charging resistors, trigger inductors, etc.). Capacitors are connected in pairs via a spark gap switch, forming LTD "bricks" [9]. The top and bottom capacitors in each brick are charged to opposite polarities (up to $\pm$100 kV for BLUE). Each BLUE cavity consists of ten bricks, which will discharge into a central coaxial transmission line. The discharge is expected to produce a current pulse that rises from 0 to 150 kA in $\sim$100 ns into a matched load.

Fig. 8(b) depicts a computer-aided design (CAD) model of the four BLUE cavities stacked together in series and connected to a GW-class MILO (labeled "HPM load"). By varying the number of cavities used, the performance of the MILO can be characterized as a function of the injected voltage up to 800 kV, similar to what was studied numerically in Fig. 5.

Fig. 8(c) depicts the brazed, GW-class MILO to be tested at UM. Experiments testing the effects of varied injected voltage and the application of external magnetic fields on the MILO's performance await the completion of the BLUE facility.

VI. Conclusion

A GW-class MILO was simulated in HFSS and CST. HFSS was used to find the dispersion characteristics of the SWS, examine potential operating modes, and compare two different methods for mode identification in cold test simulation. The particle-in-cell (PIC) software CST-PS was used to reproduce previous experimental data [16] and predict power output as a function of the injected voltage. It was determined that CST-PS had difficulty resolving a consistent operating mode at

Authorized licensed use limited to: University of Michigan Library. Downloaded on May 12,2020 at 14:57:26 UTC from IEEE Xplore. Restrictions apply.

This article has been accepted for inclusion in a future issue of this journal. Content is final as presented, with the exception of pagination.

higher injected voltages, but the output power observed when the TM_{01} π-mode dominated agreed with expectations. The CST-PS model was used to consider the effects of an externally applied axial magnetic field on a GW-class MILO. The MILO was immersed in a uniform, purely axial field, and it was concluded that the application of this field is not intrinsically harmful to microwave generation so long as the axial flow velocity is properly synchronized with the SWS phase velocity. Finally, experimental preparations are now well underway for testing a brazed GW-class MILO on the BLUE LTD facility at UM.

REFERENCES

[1] M. C. Clark, B. M. Marder, and L. D. Bacon, "Magnetically insulated transmission line oscillator," *Appl. Phys. Lett.*, vol. 52, no. 1, pp. 78–80, Jan. 1988.

[2] B. M. Marder, "Simulated behavior of the magnetically insulated oscillator," *J. Appl. Phys.*, vol. 65, no. 3, pp. 1338–1349, Feb. 1989.

[3] J. W. Eastwood, K. C. Hawkins, and M. P. Hook, "The tapered MILO," *IEEE Trans. Plasma Sci.*, vol. 26, no. 3, pp. 698–713, Jun. 1998.

[4] R. W. Lemke, S. E. Calico, and M. C. Clark, "Investigation of a load-limited, magnetically insulated transmission line oscillator (MILO)," *IEEE Trans. Plasma Sci.*, vol. 25, no. 2, pp. 364–374, Apr. 1997.

[5] M. D. Haworth *et al.*, "Significant pulse-lengthening in a multigigawatt magnetically insulated transmission line oscillator," *IEEE Trans. Plasma Sci.*, vol. 26, no. 3, pp. 312–319, Jun. 1998.

[6] R. W. Lemke, J. W. Luginsland, and M. D. Haworth, "Evidence of a new pulse-shortening mechanism in a load-limited MILO," *IEEE Trans. Plasma Sci.*, vol. 28, no. 3, pp. 511–516, Jun. 2000.

[7] G. B. Collins, *Microwave Magnetrons*. New York, NY, USA: McGraw-Hill, 1948.

[8] R. J. Barker and E. Schamiloglu, *High-Power Microwave Sources and Technologies*. New York, NY, USA: IEEE Press, 2001.

[9] R. D. McBride *et al.*, "A primer on pulsed power and linear transformer drivers for high energy density physics applications," *IEEE Trans. Plasma Sci.*, vol. 46, no. 11, pp. 3928–3967, Nov. 2018.

[10] B. M. Koval'chuk *et al.*, "Fast primary storage device utilizing a linear pulse transformer," *Russian Phys. J.*, vol. 40, no. 12, pp. 1142–1153, Dec. 1997.

[11] A. A. Kim *et al.*, "Development and tests of fast 1-MA linear transformer driver stages," *Phys. Rev. Special Topics-Accel. Beams*, vol. 12, no. 5, May 2009, Art. no. 050402.

[12] A. A. Kim *et al.*, "Review of high-power pulsed systems at the Institute of high current electronics," *Matter Radiat. Extremes*, vol. 1, no. 4, pp. 201–206, Jul. 2016.

[13] S. Portillo, A. Kuskov, S. Horne, J. Lehr, and E. Schamiloglu, "Initial characterization of a modular magnetically insulated line oscillator," in *Proc. IEEE 41st Int. Conf. Plasma Sci. (ICOPS) IEEE Int. Conf. High-Power Part. Beams (BEAMS)*, Washington, DC, USA, May 2014, p. 1.

[14] Y. Fan, X. Wang, G. Li, H. Yang, H. Zhong, and J. Zhang, "Experimental demonstration of a tunable load-limited magnetically insulated transmission line oscillator," *IEEE Trans. Electron Devices*, vol. 63, no. 3, pp. 1307–1311, Mar. 2016.

[15] Y. Yu, X. Wang, Y. Fan, A. Li, and S. Li, "Design of a dual-band radiation system for a complex magnetically insulated line oscillator," *AIP Adv.*, vol. 8, no. 5, May 2018, Art. no. 055212.

[16] M. D. Haworth *et al.*, "Recent progress in the hard-tube MILO experiment," *Proc. SPIE*, vol. 3158, pp. 28–39, Oct. 1997.

[17] X. Gao *et al.*, "Dispersion characteristics of a slow wave structure with metal photonic band gap cells," *Nucl. Instrum. Methods Phys. Res. A, Accel. Spectrom. Detect. Assoc. Equip.*, vol. 592, no. 3, pp. 292–296, Jul. 2008.

[18] B. McCowan, "Calculating slow-wave circuit parameters with HFSS," in *Proc. Abstracts. Int. Vac. Electron. Conf.*, Monterey, CA, USA, May 2000, p. 2.

[19] P. J. Christenson, D. P. Chernin, A. L. Garner, and Y. Y. Lau, "Resistive destabilization of cycloidal electron flow and universality of (near-) Brillouin flow in a crossed-field gap," *Phys. Plasmas*, vol. 3, no. 12, pp. 4455–4462, Dec. 1996.

[20] P. Zhang, Á. Valfells, L. K. Ang, J. W. Luginsland, and Y. Y. Lau, "100 years of the physics of diodes," *Appl. Phys. Rev.*, vol. 4, no. 1, Mar. 2017, Art. no. 011304.

[21] S. E. Calico, M. C. Clark, R. W. Lemke, and M. C. Scott, "Experimental and theoretical investigations of a magnetically insulated line oscillator (MILO)," *Proc. SPIE*, vol. 2557, pp. 50–59, Sep. 1995.

[22] J. Leckbee *et al.*, "Linear Transformer Driver (LTD) research for radiographic applications," in *Proc. IEEE Pulsed Power Conf.*, Chicago, IL, USA, Jun. 2011, pp. 614–618.

[23] J. J. Leckbee *et al.*, "Commissioning and power flow studies of the 2.5-MeV ursa minor LTD," in *Proc. IEEE Int. Power Modulator High Voltage Conf. (IPMHVC)*, San Diego, CA, USA, Jun. 2012, pp. 169–173.

[24] B. M. Kovalchuk, S. D. Polevin, R. V. Tsygankov, and A. A. Zherlitsyn, "S-band coaxial vircator with electron beam premodulation based on compact linear transformer driver," *IEEE Trans. Plasma Sci.*, vol. 38, no. 10, pp. 2819–2824, Oct. 2010.

Drew A. Packard (Graduate Student Member, IEEE) received the B.S.E. and M.S.E. degrees in nuclear engineering and radiological sciences from the University of Michigan, Ann Arbor, MI, USA, in 2016 and 2017, respectively.

As a graduate student, he performs research on high-power microwave devices under the mentorship of Prof. Gilgenbach with the Plasma, Pulsed Power, and Microwave Laboratory (PPPML), University of Michigan, he specializes in crossed field devices. During his time with PPPML, he has simulated, designed, and tested magnetrons, crossed field amplifiers, and magnetically insulated line oscillator's. He has completed two internships with L-3 Communications, Electron Devices Division, San Carlos, CA, USA. His general research interests include charged particle beams, accelerators, diode physics, beam-wave interaction, radio frequency (RF) sources and engineering, antennas, high-power microwaves, pulsed power, simulation techniques, and general electromagnetic phenomena.

Anna Cooleybeck received the B.S.E. degree in engineering physics with a focus on plasma physics from the University of Michigan (UM), Ann Arbor, MI, USA, in 2020. She is currently pursuing the Ph.D. degree in physics from the University of Wisconsin–Madison, Madison, WI, USA.

She was an Undergraduate Research Assistant with the Plasma, Pulsed Power, and Microwave Laboratory, UM, where she worked on modeling microwave devices.

Nicholas M. Jordan (Senior Member, IEEE) received the B.S.E., M.S.E., and Ph.D. degrees in nuclear engineering and radiological science from the University of Michigan, Ann Arbor, MI, USA, in 2002, 2004, and 2008, respectively.

From 2008 to 2013, he was with Cybernet Systems Corporation, Ann Arbor, where he developed technology to disable uncooperative vehicles using microwave pulses. He is currently an Associate Research Scientist with the Plasma, Pulsed Power, and Microwave Laboratory, University of Michigan. His current research interests include high-power microwave devices, pulsed power, laser ablation, Z-pinch physics, and plasma discharges.

Authorized licensed use limited to: University of Michigan Library. Downloaded on May 12,2020 at 14:57:26 UTC from IEEE Xplore. Restrictions apply.

This article has been accepted for inclusion in a future issue of this journal. Content is final as presented, with the exception of pagination.

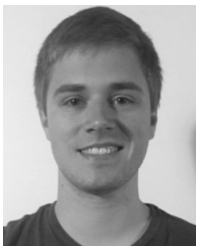

Brendan J. Sporer received the undergraduate dual degree in nuclear and mechanical engineering, in 2017, from Penn State University, State College, PA, USA. He is currently pursuing the Ph.D. degree with the University of Michigan, Ann Arbor, MI, USA, under the supervision of Dr. Ryan McBride.

His research focuses on the construction of a new pulsed power system based on linear transformer driver (LTD) technology with the Plasma, Pulsed Power, and Microwave Laboratory, University of Michigan. LTDs are critical for the next generation of petawatt-class accelerators for high-yield inertial fusion. His research interests lie in controlled fusion and nuclear powered/propelled spacecraft.

Alexander E. Mazarakis, photograph and biography not available at the time of publication.

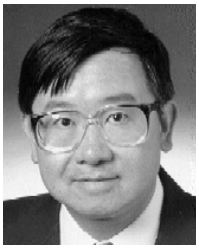

Y. Y. Lau (Fellow, IEEE) received the B.S., M.S., and Ph.D. degrees in electrical engineering from the Massachusetts Institute of Technology, Cambridge, MA, USA, in 1968, 1970, and 1973, respectively.

He is currently a Professor with the University of Michigan, Ann Arbor, MI, USA, where he is also specialized in radio frequency (RF) sources, heating, and discharge.

Dr. Lau was an Elected Fellow of the American Physical Society in 1986. He received the 1999 IEEE Plasma Science and Applications Award and the 2017 IEEE John R. Pierce Award for Excellence in vacuum electronics. He served three terms as an Associate Editor for the *Physics of Plasmas* from 1994 to 2002.

Ronald M. Gilgenbach (Life Fellow, IEEE) received the B.S. and M.S. degrees from the University of Wisconsin—Madison, Madison, WI, USA, in 1972 and 1973, respectively, and the Ph.D. degree in electrical engineering from Columbia University, New York, NY, USA, in 1978.

He spent several years as a member of the Technical Staff with Bell Telephone Labs, Holmdel, NJ, USA, in the mid-1970s. From 1978 to 1980, he performed gyrotron research with the Naval Research Laboratory, Washington, DC, USA, and also performed the first electron cyclotron heating experiments on tokamak plasma in the USA with the Oak Ridge National Laboratory, Oak Ridge, TN, USA. He joined the University of Michigan (UM), Ann Arbor, MI, USA, in 1980, as a Faculty Member, where he became the Director of the Plasma, Pulsed Power and Microwave Laboratory. He has supervised 51 graduated Ph.D. students with UM. He has collaborated in research with scientists at the Air Force Research Laboratory, Kirtland AFB, Albuquerque, NM, USA; Sandia National Laboratories, Albuquerque, NM, USA; NASA Glenn Research Center, Cleveland, OH, USA; Northrop Grumman Corporation, Rolling Meadows, IL, USA; L-3 Communications, Williamsport, PA, USA; General Motors Research Laboratories; Warren, MI, USA, the Los Alamos National Laboratory, Los Alamos, NM, USA; Fermilab, Batavia, IL, USA; the U.S. Naval Research Laboratory, Washington; and the Institute of High Current Electronics, Tomsk, Russia. He is currently the Chihiro Kikuchi Collegiate Professor with the Department of Nuclear Engineering and Radiological Sciences, UM. He has authored or coauthored some 200 articles in refereed journals and books and holds five patents granted.

Dr. Gilgenbach is a fellow of the American Physical Society Division of Plasma Physics. He was a recipient of the NSF Presidential Young Investigator Award in 1984, the Plasma Sciences and Applications Committee (PSAC) Award from the IEEE in 1997, and the Peter Haas Pulsed Power Award from IEEE in 2017. He served as the IEEE PSAC Chair from 2007 to 2008. He was an Associate Editor of the *Physics of Plasmas* journal.

Ryan D. McBride (Member, IEEE) received the Ph.D. degree from Cornell University, Ithaca, NY, USA, in 2009.

He conducted experimental research using the 1-MA COBRA pulsed-power facility to generate and study high-power x-ray sources at Cornell University. From 2008 to 2016, he was with the Sandia National Laboratories, Albuquerque, NM, USA, where he held appointments as a Staff Physicist and the Department Manager. At Sandia, he conducted research in nuclear fusion, high-power radiation generation, and high-pressure material properties using the 25-MA Z-pulsed-power facility. He is currently an Associate Professor with the Department of Nuclear Engineering and Radiological Sciences, University of Michigan, Ann Arbor, MI, USA. His current research interests include plasma physics, nuclear fusion, high-power radiation generation, pulsed-power technology, and diagnostics. His research is conducted primarily within the University of Michigan's Plasma, Pulsed Power, and Microwave Laboratory, which includes the BLUE linear transformer driver facility (150 kA, 100–800 kV, and 100 ns). BLUE is presently being prepared to drive novel high-power microwave sources.

Authorized licensed use limited to: University of Michigan Library. Downloaded on May 12,2020 at 14:57:26 UTC from IEEE Xplore. Restrictions apply.